Geological Survey of Japan Cruise Report No. 18, p. 224–230, 1982

VIII. MANGANESE NODULES OF THE WAKE-TAHITI TRANSECT: A RELATIONSHIP BETWEEN COVERAGE AND ABUNDANCE

Takayuki Saito and Katsuya Tsurusaki**

Introduction

The observation and measurement of manganese nodule samples and deep-sea photographs were conducted on board for the purpose of collecting basic data to obtain quantitative relationship between nodule dimention and its weight, to estimate nodule abundance from deep-sea photographs, and to obtain magnitude of impact against various kinds of deep-sea bottom sediments. They include: 1) sizing, weighing of sampled nodules and calculation of nodule abundance, 2) measurements of long axis, short axis, thickness and weight of each nodule at some stations, 3) photographing deep sea floor using an one-shot-camera and calculation of nodule coverage, and 4) measurements of impact to alight on deep-sea bottom with a small mechanical recorder in a glass sphere of the free fall grab at some stations.

Procedure and equipment

Manganese nodules sampled by three kinds of sampler, a single spade box corer, a double spade box corer, and a freefall grab, were classified into prearranged size fractions.

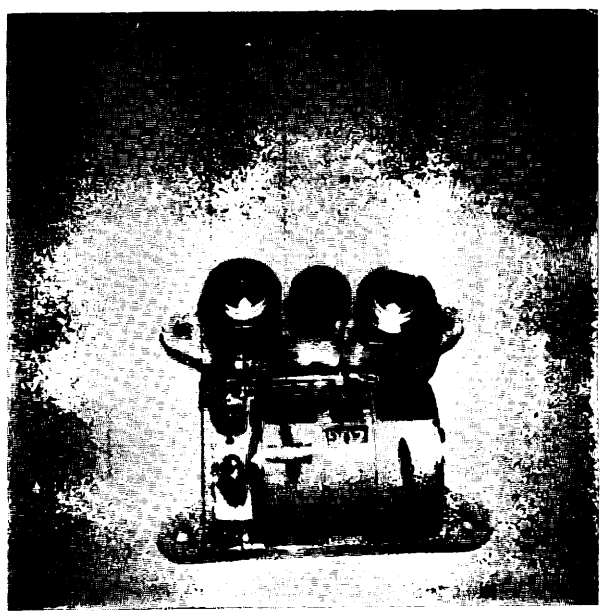

Fig. VIII-1 A small mechanical acceleration recorder used for measurement of magnitude of impact by freefall grab's alighting on the sea floor.

*National Research Institute for Pollution and Resources, Tsukuba.

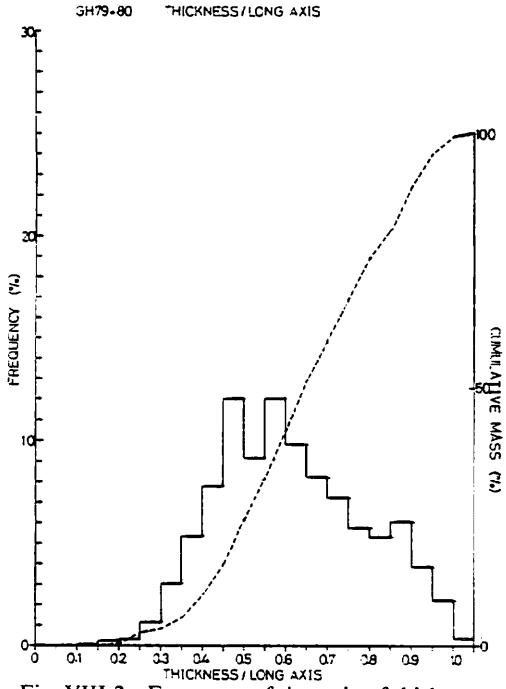

Fig. VIII-2 Frequency of the ratio of thickness to long axis of nodules (for all the types) collected in GH79–1 and GH80–1 cruises. Data source for the GH79–1 nodules: HANDA and TSURUSAKI (1981).

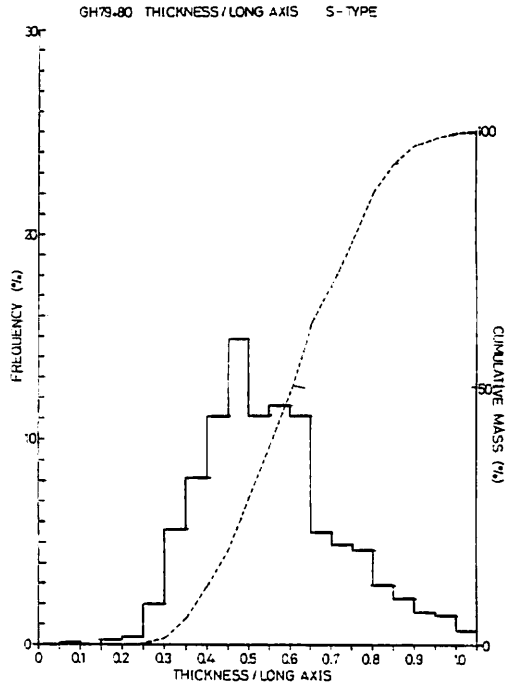

Fig. VIII-3 Frequency of the ratio of thickness to long axis of s-type nodules collected in GH79–1 and GH80–1 cruises.

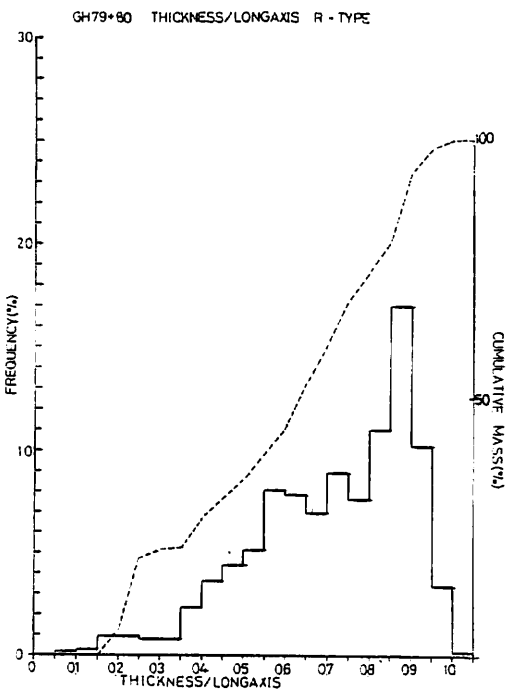

Fig. VIII-4 Frequency of the ratio of thickness to long axis of r-type nodules collected in GH79–1 and GH80–1 cruises.

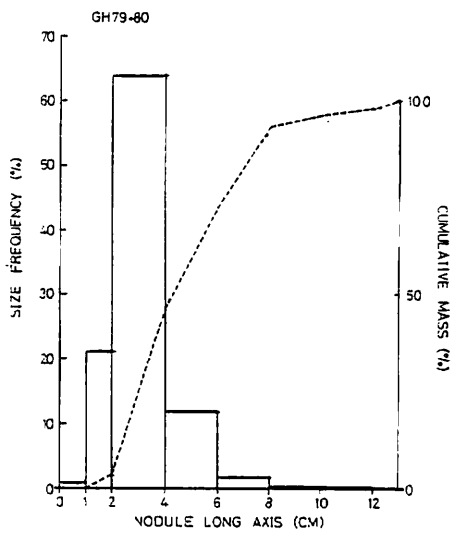

Fig. VIII-5 Frequency of size of long axis of nodules (for all the types) collected in GH79–1 and GH80–1 cruises.

After sizing, their weight was measured using a balance and they were counted up at respective size fractions. At some stations, long axis, short axis, and thickness of each nodule were measured using a slide caliper, and its weight was also measured using a shipboard electrical balance.

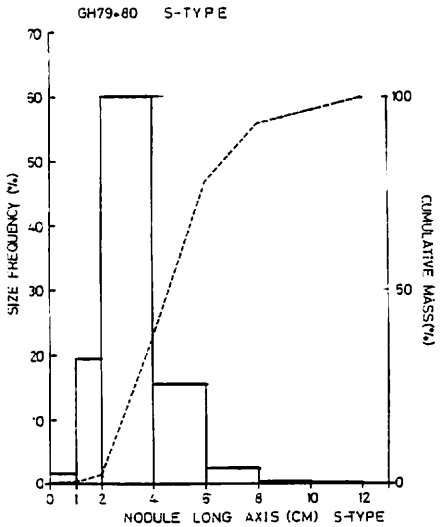

Fig. VIII-6 Frequency of size of long axis of s-type nodules collected in GH79–1 and GH 80–1 cruises.

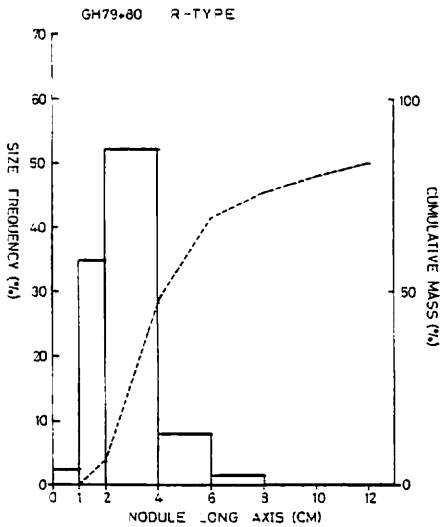

Fig. VIII-7 Frequency of size of long axis of r-type nodules collected in GH79–1 and GH 80–1 cruises.

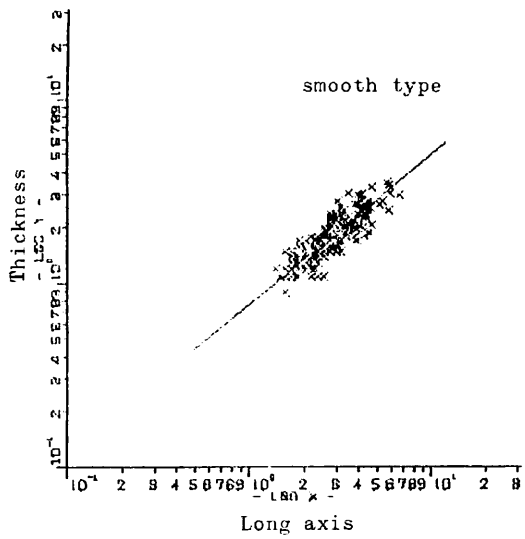

Fig. VIII-8 Relationship between long axis and thickness of s-type nodules from St. 1596 (FG198–3; abundance 21.0 kg/m^2, coverage 40%).

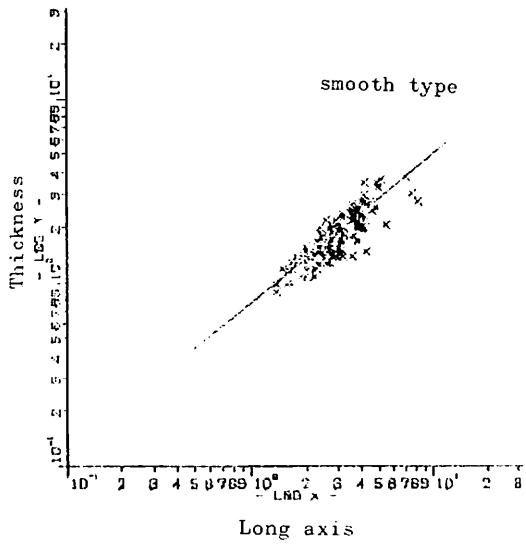

Fig. VIII-9 Relationship between long axis and thickness of s-type nodules from St. 1596 (FG198–4; abundance 19.6 kg/m^2, coverage 405).

An one-shot-camera used consisted of 16 mm still camera, flash bulb, battery, and trigger, and they were mounted in a cylindrical pressure case about 23 cm long by 9 cm in diameter. It was attached to inside of a freefall grab and could take a picture of the sea floor just before sampling by the function of the trigger.

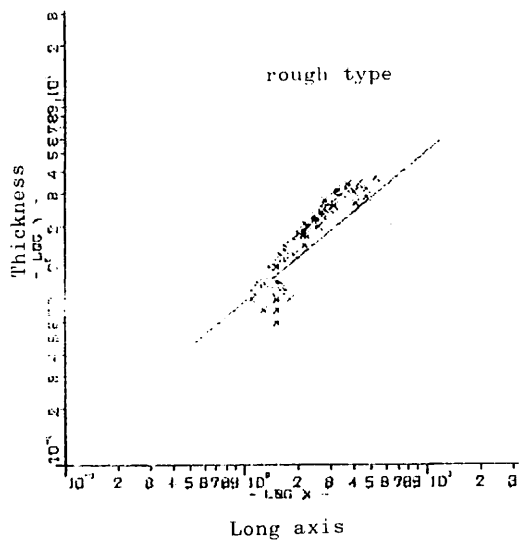

Fig. VIII-10 Relationship between long axis and thickness of r-type nodules from St. 1601 (FG203–2; abundance 8.3 kg/m², coverage 1%).

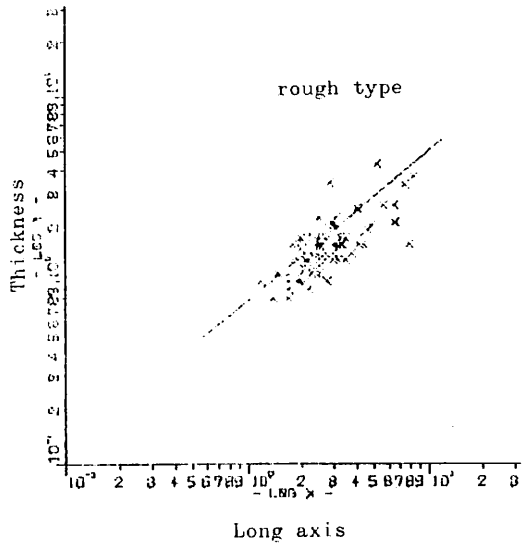

Fig. VIII-11 Relationship between long axis and thickness of r-type nodules from St. 1619 (FG222–1; abundance 12.8 kg/m², coverage 15%).

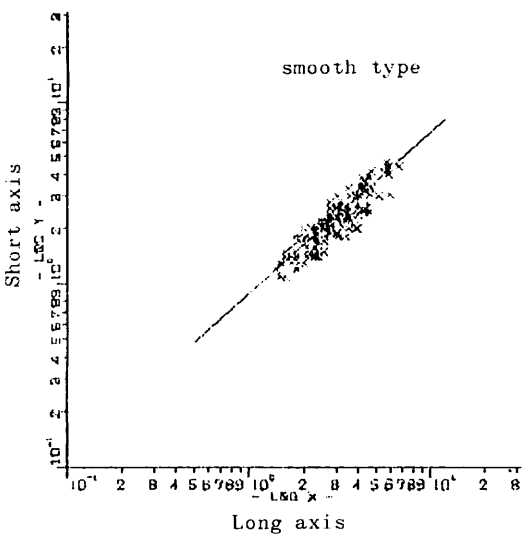

Fig. VIII-12 Relationship between long axis and short axis of nodules (s-type) from St. 1596 (FG198–3).

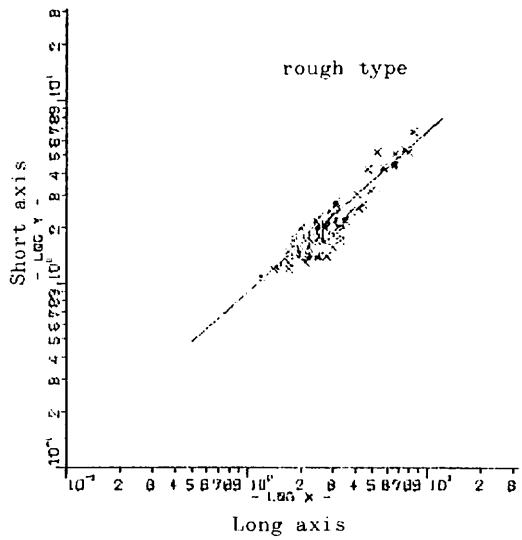

Fig. VIII-13 Relationship between long axis and short axis of nodules (r-type) from St. 1619 (FG222–1).

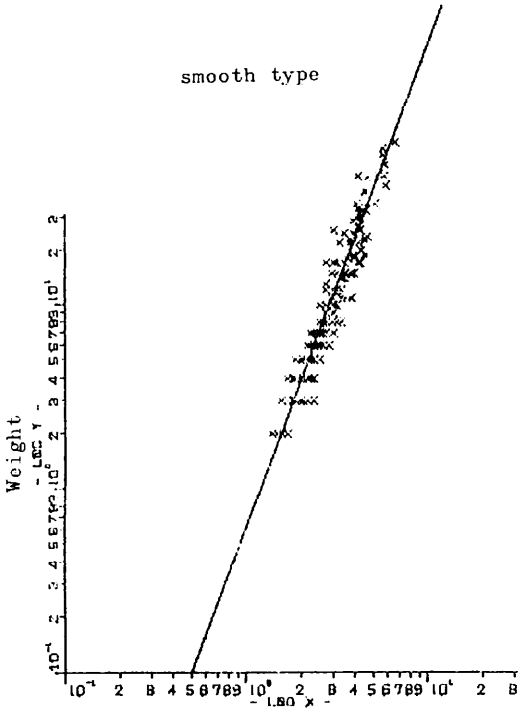

Fig. VIII-14 Relationship between wet weight and long axis of nodules (s-type) from St. 1596 (FG198–3).

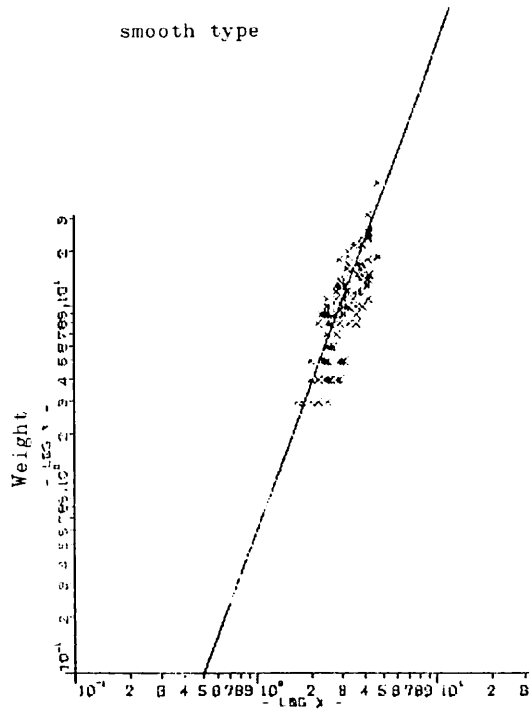

Fig. VIII-15 Relationship between wet weight and long axis of nodules (s-type) from St. 1607 (FG209–2).

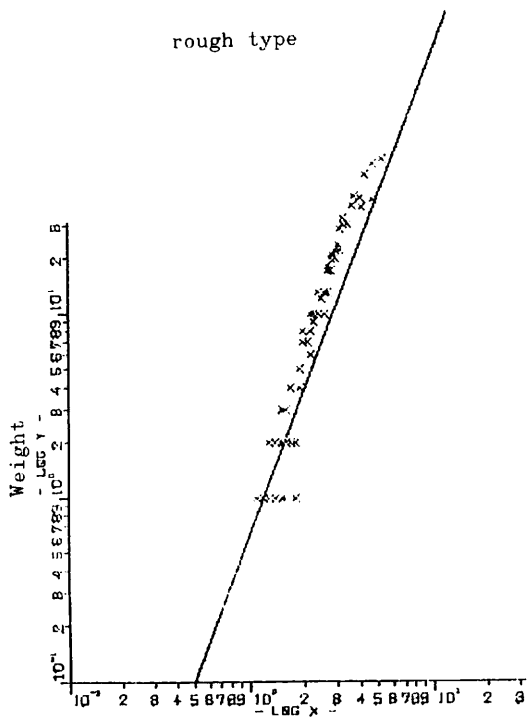

Fig. VIII-16 Relationship between wet weight and long axis of nodules (r-type) from. St. 1601 (FG203–2).

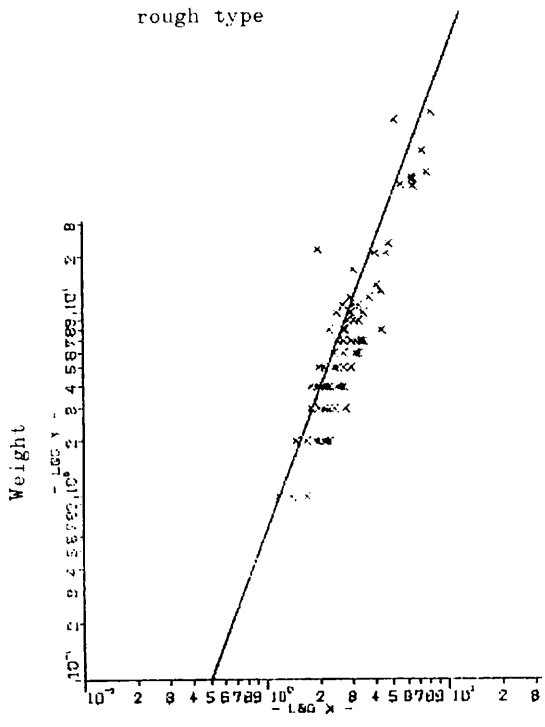

Fig. VIII-17 Relationship between wet weight and long axis of nodules (r-type) from St. 1619 (FG222–1).

Magnitude of impact by freefall grab's alighting on the deep-sea floor was measured with a small mechanical acceleration recorder with a capability of measuring maximum 20 g acceleration (Fig. VIII-1), which was fixed with in a glass sphere used as a buoy of a freefall grab.

Preliminary results

Figure VIII-2 shows a frequency of the ratio of thickness to long axis of nodules measured during both the GH79–1 (data source = HANDA and TSURUSAKI, 1980) and the GH80–1 research cruises. Figures VIII-3 and VIII-4 also show the relationship between them, but concerning s-type nodules and r-type ones respectively. Figures VIII-5 to VIII-7 show size frequency of long axis of nodules. Examples of the relationship between long axis and thickness of nodules collected in a single freefall grab are illustrated in Figures VIII-8 to VIII-11 with logarithmic graphs. The data on the other site also show the same results.

All the available data show that the relation between thickness and long axis of the nodules can be expressed as an equation (1).

$$(\text{Thickness}) = 0.76(\text{Long axis})^{0.82} \qquad (1)$$

Then Figs VIII-12 and VIII-13 show the relationship between long axis and short axis of nodules plotted on logarithmic graphs. This relationship is expressed as an equation (2) as well as the relationship between long axis and thickness.

$$(\text{Short axis}) = 0.88(\text{Long axis})^{0.91} \qquad (2)$$

Table VIII-1 Nodule abundance estimated from deep sea photographs.

	actual	estimated*	agreement
FG196–4	27.6 kg/m^2	25.1 kg/m^2	9%
B14	18.3 kg/m^2	22.2 kg/m^2	21%

*calculated values using the equation (3).

Table VIII-2 Magnitude of impact acceleration.

St. No.	abundance (kg/m^2)	coverage (%)	upward acceleration (g)	downward ac.
1589	—	60	5.5	3.0
1591	0	0	2.5	5.7
1599	—	0	3.6	5.0
1604	0	0	2.2	2.7
1606	—	5	4.0	1.6
1607	11.6	30	5.6	2.5
1620	26.1	40	4.6	0.5
1623	0	0	4.0	1.0
1629	7.0	0	4.8	1.2
1631	10.4	5	4.5	2.3
1633	0	0	2.6	3.6
1635	5.0	5	4.0	1.8
1643	21.8	70	3.7	3.0
1645	23.4	80	4.2	6.7
1646	7.2	40	10.0	7.2

—no sampling.

Figures VIII-14 to VIII-17 illustrate the relationship between long axis and weight of nodules plotted on logarithmic graphs. The relationship can be expressed as the following power equation.

$$(\text{Weight}) = 0.65(\text{Long axis})^{2.70} \quad (3)$$

Nodule abundance was estimated from deep-sea photographs based on the above relationship(equation-3). These estimates were compared to actual nodule abundance, and agreement of the two value was almost within 20% (Table VIII-1).

Magnitude of impact by freefall grab's alighting on the deep-sea floor measured with a small mechanical recorder was listed in Table VIII-2. The relationship between the magnitude of impact and the state of sea floor has not been sufficiently characterized yet. Further investigations and analyses are needed for this problem.

Reference

HANDA, K. and TSURUSAKI, K. (1981) Manganese nodules: relationship between coverage and abundance in the northern part of Central Pacific Basin. *In* MIZUNO, A. (*ed.*), *Geol. Surv. Japan Cruise Rept.*, no. 15, p. 184–217.